Research Square

Preprints are preliminary reports that have not undergone peer review.
They should not be considered conclusive, used to inform clinical practice,
or referenced by the media as validated information.

Uncertainties in the Evolution of South Indian Ocean Subsurface Heat Content in CMIP6 models: The Role of the Indonesian Throughflow and Its Pacific Drivers

SAJIDH CK

sajidh.c.k@gmail.com

Indian Institute of Technology Madras https://orcid.org/0009-0002-1589-0635

Salma Jasmine

ESSO- Indian National Centre for Ocean Information Services

Abhisek Chatterjee

ESSO- Indian National Centre for Ocean Information Services

Research Article

Keywords: Ocean heat content, Indonesian throughflow, ENSO, CMIP6, Internal variability

Posted Date: March 18th, 2026

DOI: https://doi.org/10.21203/rs.3.rs-9063624/v1

License: This work is licensed under a Creative Commons Attribution 4.0 International License.
Read Full License

Uncertainties in the Evolution of South Indian Ocean Subsurface Heat Content in CMIP6 models: The Role of the Indonesian Throughflow and Its Pacific Drivers

Sajidh C K[1,2,3*], Salma Jasmine[1] and Abhisek Chatterjee[1]

[1]*Indian National Centre for Ocean Information Services, Ministry of Earth Sciences, Hyderabad, India*.

[2]*KUFOS-INCOIS Joint Centre, Kerala University of Fisheries and Ocean Studies, Kochi, India*.

[3]*Indian Institute of Technology Madras, Chennai, India.*

**Corresponding author: Sajidh C K (sajidh.c.k@gmail.com); ORCID ID: 0009-0002-1589-0635*

Abstract

The Subtropical Indian Ocean (STIO) has emerged as a prominent warming hotspot since the 1950s under anthropogenic forcing. However, coupled climate models have struggled to reproduce the observed spatial distribution and magnitude of this warming. An analysis using 30 CMIP6 models reveals that the largest inter-model uncertainty in long-term ocean heat uptake over the STIO. In this study, we investigate the causes of this spread, primarily focusing on the role of the Indonesian Throughflow (ITF) and its Pacific linkages. CMIP6 models exhibit large inconsistencies in simulating ITF induced upper ocean (top 700 m) heat content variability in the STIO. A regression-based ITF model (ITF-PAC) using canonical ENSO and ENSO-Modoki indices broadly reproduces a similar relationship between the Pacific climate modes and the STIO heat content, but with a much stronger correlations in models than in reanalysis, suggesting an exaggerated Pacific control in the CMIP6 models. Our results highlight these coupled models possess low skill and large uncertainty in capturing ITF-driven heat content variability and long-term Pacific trends that can modulate STIO warming.

Keywords: Ocean heat content · Indonesian throughflow · ENSO · CMIP6 · Internal variability

1 Introduction

Ocean plays a pivotal role in regulating Earth's climate by absorbing nearly 90% of the excess heat generated by anthropogenic greenhouse gas emissions (Trenberth et al., 2014; Wijffels et al., 2016; Meyssignac et al., 2019; IPCC, 2021). This immense heat uptake buffers the climate system from more abrupt changes in the surface atmospheric conditions, but not without consequence such as ice-shelf melt (Rantanen et al., 2022; Oldenburg et al., 2024), sea level rise (Bindoff et al., 2007; Han et al., 2010; Church & White, 2011; Church et al., 201), marine heatwaves (Frölicher et al., 2018; Chen et al., 2024), intensified tropical cyclones (Webster et al., 2005; Bhatia et al., 2019), and slowing down the meridional overturning circulation (Pontes & Menviel, 2024; Madan et al., 2024) . Notably, the observed warming is neither spatially nor vertically uniform; instead, it exhibits distinct regional and depth-dependent patterns. The strongest warming signals are observed within the upper 2000 m, with the upper 700 m accounting for the bulk of heat storage (Cheng et al., 2017; Roemmich et al., 2015; von Schuckmann et al., 2020; Bagnell & DeVries, 2021; Gulev et al., 2021). Regionally, the Southern Ocean dominates heat uptake in the Southern Hemisphere, while the north Atlantic leads in the Northern Hemisphere (Cheng et al., 2022; Song et al., 2025).

Despite the relatively small area, the Indian Ocean plays a critical role in regulating the climate at global and regional scale. During the global warming hiatus spanning from the late 1990s to the early 2010s (Kerr, 2009; Easterling & Wehner, 2009; Kennedy et al., 2009; Hunt, 2011)– the Indian Ocean acted as a heat sink for the excess heat being transported from the Pacific Ocean (Rosen, 2015; Lee et al., 2015). This hiatus was characterized by persistently cold sea surface temperatures anomalies (SSTA) in the eastern Pacific, resembling La Niña–like conditions (Meehl et al., 2013; Kosaka & Xie, 2013; England et al., 2014). The associated strengthening of trade winds enhanced oceanic heat uptake, which is believed to have contributed to the temporary slowdown in the rate

of increase of global mean surface temperature. Despite the increased atmospheric heat flux, the Pacific subsurface remained cool, while the Indian Ocean experienced significant warming, absorbing approximately 70% of the heat absorbed during this period (Lee et al., 2015). This transport of heat from the Pacific to the Indian Ocean was facilitated predominantly by the Indonesian Throughflow (ITF), the inter-basin tropical conduit between the Indian Ocean and Pacific Ocean for exchange of warm and relatively fresher waters (Macdonald, 1993; Godfrey, 1996; Lee et al., 2002; Vranes et al., 2002; Gordon, 2005; Sprintall et al., 2014).

As an important component of the global thermohaline circulation, ITF plays a critical role in regulating the heat and water volume balances of the Indo-Pacific region (Sloyan and Rintoul, 2001; Gordon, 2005; Sprintall et al., 2014). The ITF exerts a pronounced influence on the thermocline structure and heat content of the South Indian Ocean (Dong and McPhaden, 2017; Zhang et al., 2018). The ITF waters that enter the Indian Ocean through the Indonesian seas partly feed the South Equatorial Current to get advected westward and eventually flows along the African coast to join the Agulhas Current (Godfrey and Golding, 1981; Godfrey, 1996). Model sensitivity experiments have shown that shutting off ITF transport leads to substantial changes in heat content, particularly in the western Pacific, along the west Australian coast, and in the Agulhas outflow region (Hirst and Godfrey, 1993; Qu et al., 1994). Notably, a significant portion of the heat carried by the ITF is released to the atmosphere over the Indian Ocean (Vranes et al., 2002). Being strongly coupled with ENSO and the equatorial trade winds, the ITF exhibits anomalously strong (weak) transports during La Niña (El Niño) periods (Feng et al., 2018). Nevertheless, Coupled model studies project significant changes in ITF transport under a warmer global climate (Sen Gupta et al., 2016; Stellema et al., 2019), which can have critical implications for the Indo-Pacific and the global climate system (Li et al., 2018; Hu et al., 2019). However, despite these projections, a comprehensive assessment of the fidelity of these coupled models in reproducing ITF dynamics and its influence on the Indian Ocean remains absent.

The Indian Ocean has experienced intermittent phases of decadal to multi-decadal cooling since the 1960s, followed by a recent warming phase characterized by rapid heat accumulation (Li et al., 2018; Sajidh et al., 2025). These warming and cooling phases are closely associated with phase transitions of the Interdecadal Pacific Oscillation (IPO) (Li et al., 2018). On decadal timescales, the Pacific influences the southern tropical and subtropical Indian Ocean by modulating surface winds over the southeastern Indian Ocean and by altering the ITF, thereby impacting regional climate variability (Jin et al., 2018a,b). While wind-driven convergence is a crucial local driver of subsurface heat accumulation in the Southern Indian Ocean, the potential role of Pacific teleconnections, particularly via the ITF, cannot be overlooked. Since the tropical Pacific is known as the pacemaker of the global climate, changes in its long-term trends can have far-reaching impacts on the global climate system, including the Indian Ocean. In this context, a recent study by Jiang et al. (2024) identified a distinct Pacific warming pattern with atmospheric and oceanic signatures that are different from those associated with the IPO, suggesting additional modes of low-frequency Pacific variability that may influence the Indian Ocean.

Since coupled climate models are routinely employed to project the future evolution of the Earth system, a fidelity check of their representation of Indo-Pacific teleconnections, long-term Pacific trends, and their potential impacts on South Indian Ocean heat content is necessary. A recent study reports a large spread in CMIP6 model behaviour in representing surface temperature trends during the hiatus period (Soumya, 2025). However, the role of subsurface heat transport through the ITF in shaping variability in the South Indian Ocean remains poorly assessed. Given that the ITF facilitates the sequestration of heat into the deeper layers of the South Indian Ocean, this study examines how CMIP6 models represent decadal upper ocean heat content variability (up to 700 m of the water column). We focus on ITF-driven heat content variability in the South Indian Ocean, the representation of Indo-Pacific teleconnections, and the long-term Pacific trends that influence South Indian Ocean climate. In particular, the role of the ITF in regulating South Tropical Indian Ocean heat content, and the extent to which its upstream Pacific drivers are realistically represented across climate model ensembles, remain insufficiently examined. The rest of this paper is organized as follows: Section 2 describes the datasets and methods, Section 3 presents the main results, and Section 4 summarizes the findings.

2 Data and Methods

2.1 Data

We use historical simulations from 30 CMIP6 models (Table 1), focusing on potential temperature (thetao), sea surface temperature (tos), sea surface height above the geoid (zos), and zonal wind stress (tauu) for the historical simulation spanning the period 1850-2014. To ensure equal representation, we select a single realization per model, primarily r1i1p1f1. To compute dynamic sea level (DSL) the global mean from the respective model is removed, following Gregory et al. (2019) and Griffies et al. (2016). All model outputs are then uniformly regridded to a 1°×1° resolution.

For an observational reference, we use Ocean Reanalysis System 4 (ORAS4) provided by the European Centre for Medium-Range Weather Forecasts (ECMWF) (Balmaseda et al. 2013) with a 1°×1°horizontal resolution spanning the period of 1958–2017. ORAS4 provides a more realistic estimate of the Indonesian Throughflow (ITF), with a full-depth mean transport of approximately 13 Sv. We choose ORAS4 over Ocean Reanalysis System 5 (ORAS5; Zuo et al. 2019), which reports a higher mean ITF (~20 Sv) at full-depth integration. However, as shown in the earlier studies, the variability of ITF transport is similar in ORAS4 and ORAS5 (Mayer et al., 2018), and hence ORAS4 is considered more suitable for this study.

Monthly sea surface temperature is obtained from HadISST v1.1 (Rayner et al., 2003), and zonal winds from ERA5 (Hersbach et al. 2020). All datasets are analyzed over the period 1958–2014, except as mentioned otherwise, limited by the earliest availability of reanalysis records and the end year of CMIP6 historical simulations.

2.2 Methods

The ocean heat content integrated up to top 700 m of the water column (h_{700}) is calculated using the following formula

$$h_{700} = \int_0^{700} \rho \; C_p \, \theta \, dz,$$

where, θ is the potential temperature, Cp = 4096 J (kg °C)$^{-1}$ is specific heat capacity, and ρ = 1025 kg m^{-3} is seawater density.

The ITF transport is defined as the zonal velocity (*u)* integrated over the full depth of the ocean and meridionally between 24°S and 7°S at 114° E (marked in Figure 1) and is given by,

$$ITF = \int_{24°S}^{7°S} \int_{-H}^{0} u \; dz \, dy \, .$$

We assess the leading modes of Pacific variability of models using established climate indices. The Niño-3.4 index is defined as the area-averaged sea surface temperature anomaly over 5° N–5° S and 170° W–120° W, following Barnston et al. (1997), and is indicated by the solid black box in Figure 1. The El Niño Modoki Index, representing the central Pacific type of El Niño, is computed from SST anomalies as

$$\text{El Niño Modoki Index} = SSTA_{BoxA} - 0.5 \times SSTA_{BoxB} - 0.5 \times SSTAC_{BoxC,}$$

Where, Box A (165° E–140° W, 10° S–10° N), Box B (110° W–70° W, 15° S–5° N), and Box C (125° E–145° E, 10° S–20° N) denote the regions used in this study, following Ashok et al. (2009), and are shown as dashed black boxes in Figure 1.

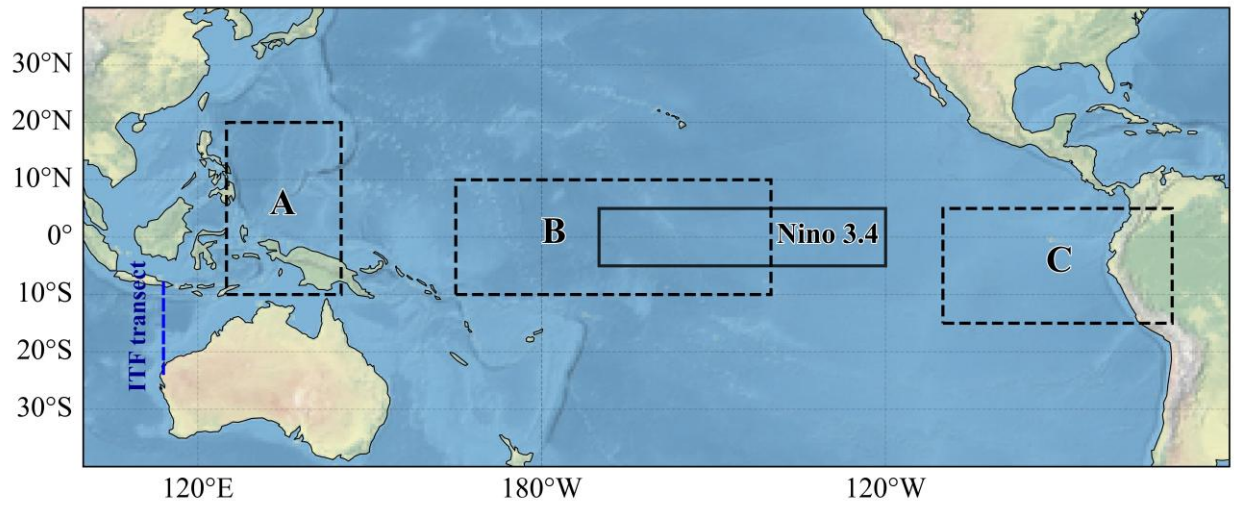


Figure 1: Climate index calculation boxes and ITF transect. The blue dashed line shows the transect used to compute the ITF. The solid black box marks the Niño-3.4 region, and the dashed black boxes denote the El Niño Modoki region.

To assess model performance across various parameters, we use the Taylor skill score (Taylor, 2001), which is given by

$$S = \frac{4(1+R)}{\left(\sigma_f+\frac{1}{\sigma_f}\right)^2 (1+R_0)},$$

where σ_f is the ratio of the spatial standard deviation of the model (σ_m) to that of the reference/observation (σ_o), and R is the pattern correlation between the model and observations. R_0 is the maximum attainable pattern correlation, which is set to 1 in this study. A higher skill score indicates better agreement between model and ORAS4.

Model name	**Institution id**	**Variant label**
ACCESS-CM2	CSIRO-ARCCSS	r1i1p1f1
ACCESS-ESM1-5	CSIRO	r1i1p1f1
BCC-CSM2-MR	BCC	r1i1p1f1
BCC-ESM1	BCC	r1i1p1f1
CESM2	NCAR	r1i1p1f1
CESM2-FV2	NCAR	r1i1p1f1
CESM2-WACCM	NCAR	r1i1p1f1
CESM2-WACCM-FV2	NCAR	r1i1p1f1
CIESM	THU	r1i1p1f1
CNRM-CM6-1	CNRM-CERFACS	r1i1p1f2
E3SM-1-0	E3SM-Project	r1i1p1f1
E3SM-1-1	E3SM-Project	r1i1p1f1
E3SM-1-1-ECA	E3SM-Project	r1i1p1f1

EC-Earth3-CC	EC-Earth-Consortium	r1i1p1f1
FGOALS-f3-L	CAS	r1i1p1f1
FGOALS-g3	CAS	r1i1p1f1
GISS-E2-1-G	NASA-GISS	r1i1p1f2
GISS-E2-1-G-CC	NASA-GISS	r1i1p1f1
GISS-E2-1-H	NASA-GISS	r1i1p1f1
HadGEM3-GC31-LL	MOHC	r1i1p1f3
INM-CM5-0	INM	r1i1p1f1
IPSL-CM6A-LR	IPSL	r1i1p1f1
MIROC6	MIROC	r1i1p1f1
MRI-ESM2-0	MRI	r1i1p1f1
NESM3	NUIST	r1i1p1f1
NorESM2-LM	NCC	r1i1p1f1
NorESM2-MM	NCC	r1i1p1f1
SAM0-UNICON	SNU	r1i1p1f1
TaiESM1	AS-RCEC	r1i1p1f1
UKESM1-0-LL	MOHC	r1i1p1f2

Table 1: List of 30 CMIP6 models used in this study

3 Results

3.1 Uncertainties in the long-term heat uptake in STIO.

The long-term trend in h_{700} from ORAS4 during 1960–2014 reveals pronounced warming in the South Tropical Indian Ocean (STIO; 45°–115°E, 15°–35°S), accompanied by significant cooling over the tropical Indian Ocean and along the west Australian coast (Figure 2a). In the North Indian Ocean both Arabian Sea and the Bay of Bengal show weaker rates of warming. The strong subsurface warming in the STIO and the cooling in the tropics has been assessed previously by different studies. For example, the observed subsurface warming in the STIO has been attributed to various factors, including the strengthening and southward migration of the subtropical gyre, as well as oceanic teleconnections from the Pacific and their temporal changes (Alory et al., 2007; Yang et al., 2020; Sajidh et al., 2025).

A similar analysis of the 30-member CMIP6 multi-model mean (MMM) reveals a different pattern for the h_{700} trend. Broadly, models fail to capture the spatial heterogeneity of the observed h_{700} trend and the strength of the warming/cooling as are observed in the ORAS4. In the STIO, the MMM exhibits a warming at a rate of 0.6×10^8 J/decade, which is about one-third of the ORAS4 based estimate (1.9×10^8 J/decade) (Figure 2b). Both ORAS4 and model trends are statistically significant at the 95% confidence level in the STIO.

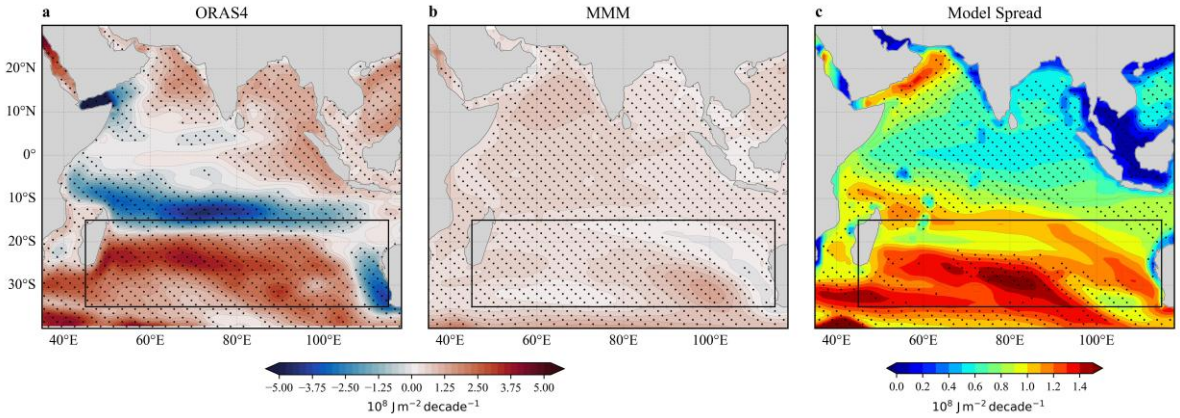


Figure 2: (a) Trend of h_{700} over 1960-2014 for ORAS4. (b) same as (a), but for the MMM. (c) Intermodel spread of the h_{700} trends among the ensembles. The stippling in (a) and (b) indicates the trends significant at 95% confidence level. The stippling in (c) represents the regions where at least 75% of the models agree on the sign of the trend.

An analysis of individual model performance helps diagnose the origin of the muted multi-model mean response and reveals substantial inter-model disagreement relative to ORAS4 (Figure S1). Eight models exhibit basin-wide positive h_{700} trends in the STIO, with models such as CIESM, FGOALS-f3-L, and FGOALS-g3 representing the upper end of the warming distribution and simulating markedly stronger warming than observed. In contrast, the remaining models show diverse trend patterns, with some models, including IPSL-CM6A-LR and NorESM2-LM, even exhibiting cooling in parts of the STIO. Figure 3 further illustrates the large spread in both the magnitude and spatial structure of h_{700} trends across models. Notably, the maximum pattern correlation between any individual model and ORAS4 does not exceed 0.6 (Figure 3), indicating only moderate agreement even for the best-performing models. These compensating warm and cool biases across models lead to substantial cancellation in the ensemble mean, thereby contributing to the weakened MMM trend and large inter-model spread in STIO.

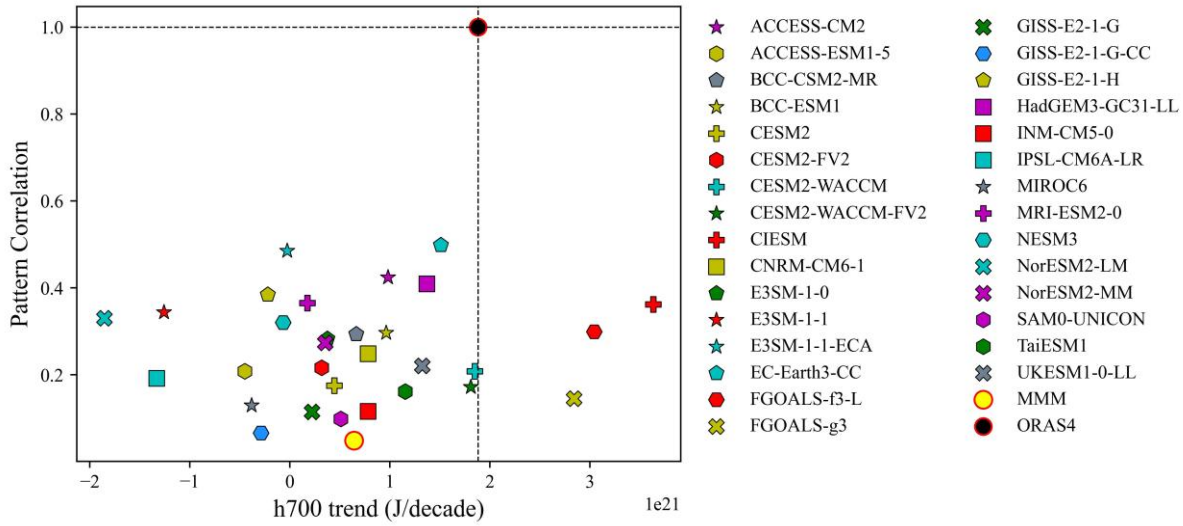


Figure 3: Scatter plot showing the relationship between decadal trends in h700 over the STIO and the corresponding pattern correlation of those trends. The x-axis represents the h700 trend, and the y-axis represents the pattern correlation. The back and yellow markers with red outlines are ORAS4 (reference) and the MMM.

To understand the vertical structure of the heat gain, Figure 4 shows zonally averaged (over 45°–115°E) temperature trends in the South Indian Ocean. While ORAS4 reveals a vertically coherent warming in the STIO extending down to ~500 m (Figure 3a), the MMM shows a more horizontally uniform yet weaker warming (Figure

4b), lacking the pronounced heterogeneity in trend across depth and latitude that is evident in ORAS4. The weaker warming trend and its spatial extent are in agreement with the inter-model spread, which exhibits a pronounced maximum between 200–600 m (Figure 4c), aligning with regions of high variability and the largest inter-model discrepancies.

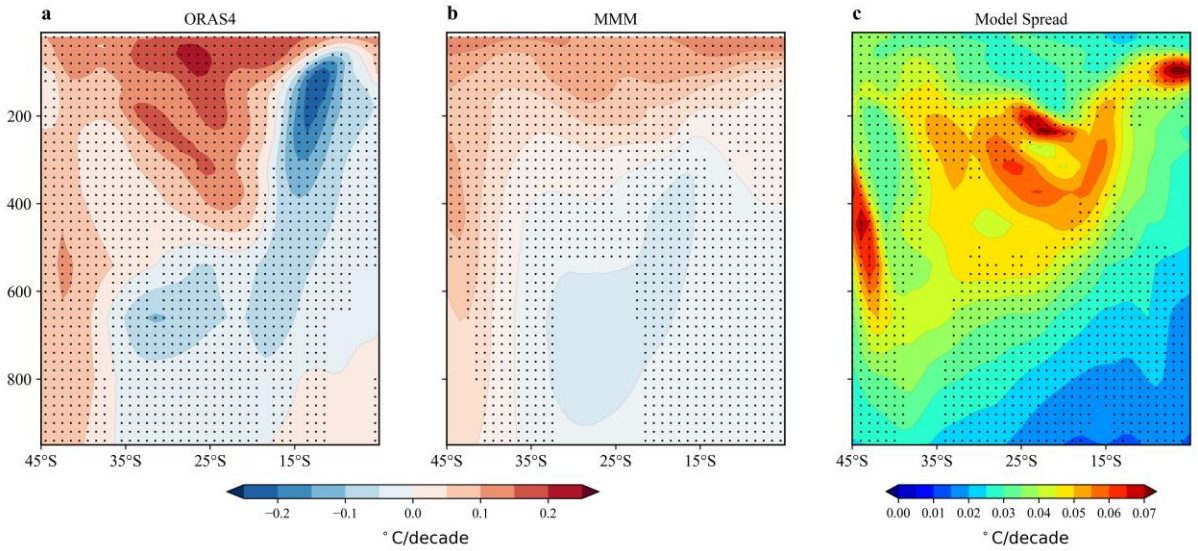


Figure 4: (a) Trend of zonally averaged temperature between 45-115°E over the period 1960-2014 for ORAS4. (b) same as a but for the MMM of model ensemble for the same period as ORAS4. (c) Intermodel spread of the zonally averaged temperature trends within the ensemble. The stippling in (a) and (b) indicates the trends significant at 95% confidence level. The stippling in (c) represents the regions where at least 75% of the models agree on the sign of the trend.

This substantial inter-model spread in STIO subsurface heat uptake motivates an evaluation of how consistently CMIP6 models represent the dominant processes governing subsurface heat evolution in the region. One such process is the ITF, which provides an important pathway linking Pacific variability to the STIO. Despite its relevance, the extent to which models capture ITF-related subsurface heat content variability on decadal timescales remains unclear. The following sections, therefore, examine how CMIP6 models represent ITF-associated variability and its implications for STIO subsurface heat content.

3.2 Representation of ITF-driven subsurface heat evolution in STIO.

Assessing the observed response of the ITF to STIO subsurface heat content (h_{700}) provides an essential benchmark before proceeding to model intercomparison. To assess this, we regress decadal ITF variability onto decadal h_{700} anomalies in the Indian Ocean at different lags using ORAS4, with h_{700} lagging the ITF to account for the delayed oceanic response (Figure 5). At zero lag, the regression reveals a strong positive response over the Southeast Indian Ocean (SEIO) and the western STIO, accompanied by a negative signal in the southern tropical band between 5° and 10° S. With increasing lag, the positive response propagates westward and intensifies, reaching a maximum at a lag of approximately four years, consistent with Dong and McPhaden (2017). The accompanying westward-propagating negative signal is likely linked to periods of enhanced ITF associated with La Niña–like conditions in the Pacific. The resulting negative wind stress curl over the SEIO can excite upwelling Rossby waves that propagate westward, giving rise to the negative subsurface signal observed in the tropical Indian Ocean (Jin et al., 2018a).

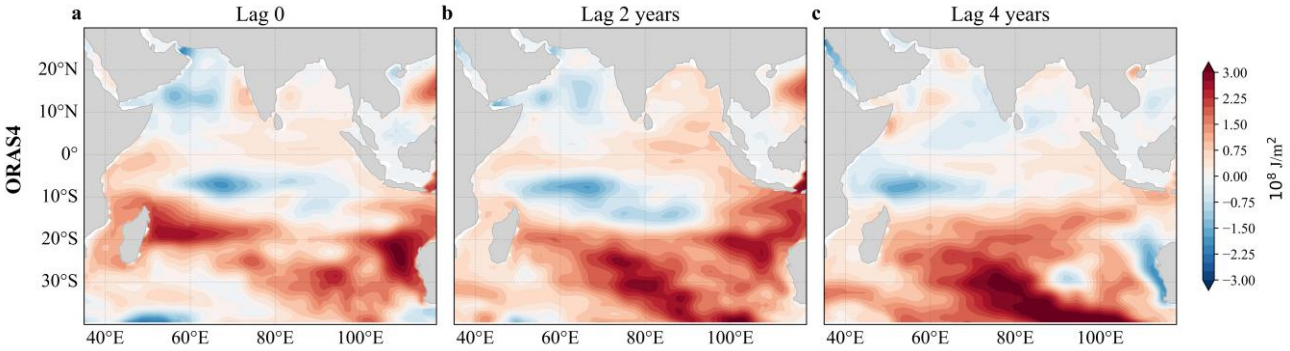


Figure 5: (a) Regression of standardised and detrended decadal ITF to detrended decadal h_{700} at zero lag, 2 year and 4-year lag (ITF leads h_{700}) for ORAS4.

Before examining the ITF - h_{700} relationship we examine the representation of the mean ITF transport in CMIP6 models. The observed ITF transport in ORAS4 during 1960–2014 is approximately 13 Sv, which is closely matched by the CMIP6 multi-model mean (~13 Sv), with an inter-model spread of about 3 Sv. Several models, BCC-CSM2-MR, BCC-ESM1, FGOALS-g3, and INM-CM4-8, simulate ITF transports below 10 Sv, while models from the GISS and NorESM families simulate transports approaching 20 Sv, highlighting the spread across the ensemble. Overall, most models perform reasonably well in capturing the mean ITF transport (Figure S2).

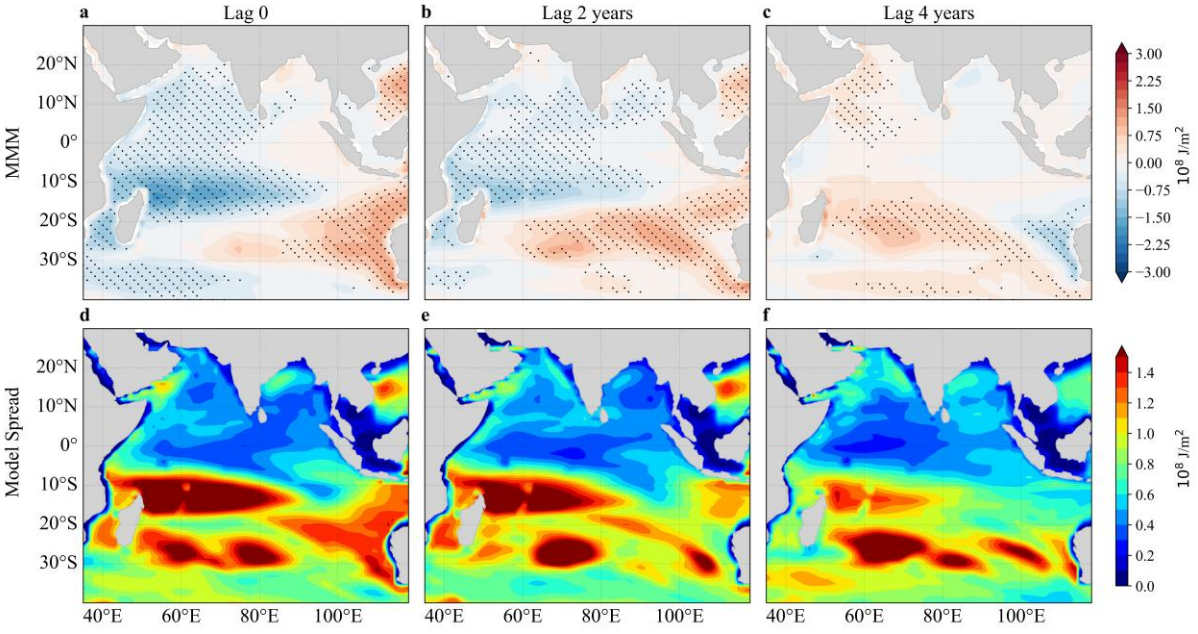


Figure 6: (a) Regression of detrended decadal ITF to detrended decadal zonally averaged (45–115°E) temperature at zero, 2-year and 4-year lags (temperature lags ITF), ITF is standardised by its own standard deviation for ORAS4. (b) Same as (a) but for the multi-model mean of the model ensemble. The stippling indicates the regions where at least 75% of the models agree on the sign of the regression coefficient. (c) Intermodel spread of the regression coefficients within the ensemble.

Applying the lead-lag regression analysis to the CMIP6 models reveals a markedly damped multi-model mean (MMM) response between ITF and h_{700} on decadal timescales (Figure 6a-c) compared to ORAS4. At zero lag, the MMM shows a dipole structure, with a positive anomaly in the SEIO and a negative anomaly in the western STIO. Unlike ORAS4, a strong positive signal is absent in the western STIO, instead a stronger negative response extending up to 90°E is present, forming a dipole-like pattern in the STIO. This negative anomaly in the western STIO may be linked to erroneous atmospheric responses to Pacific forcings in the models and warrants further

study. However, a detailed analysis of the dynamical mechanisms that caused such model discrepancies from the reanalysis is beyond the scope of the present study.

As the lag increases the MMM also shows a westward propagation of the heat to the west but the response is weak compared to ORAS4. While the signal propagates and intensifies in ORAS4, the intensification is absent for MMM. The inter-model spread of regressed heat content is largest in the western STIO at zero lag, and that decreases with increasing lag (Figure 6d-f). However, the model spread south of 20°S exhibits a propagating signal. While we do see a westward propagation, the spread averaged over the STIO (~1 × 10^8 J/m²) is almost three times the mean (~0.3 × 10^8 J/m²) of the regression coefficient over the region at almost all lags.

To examine the vertical structure of the ITF influence, we analyze lag regressions of zonally averaged temperature (45°–115°E) onto the ITF (Figure 7). In ORAS4, the warming is mostly confined to STIO latitudes, with a southward propagation of the warming cores (Figure 7a). At zero lag, the warming is confined to the upper 400 m, with cooling below. However, at a lag of four years, the warming extends deeper and farther south, without any cooling signature in the STIO, and is strictly confined north of 45°S.

In contrast, the MMM shows a much weaker and spatially diffused response (Figure 6b). The warming extends farther south than in ORAS4, lacking a clear vertical or latitudinal structure. The warming core shifts northward, with heat diffusing beyond 45°S — unlike in ORAS4. The strongest intermodel spread is confined above 400 m at all time lags (Figure 7c). This indicates a weak or misrepresented ITF-induced vertical heat redistribution in CMIP6 models.

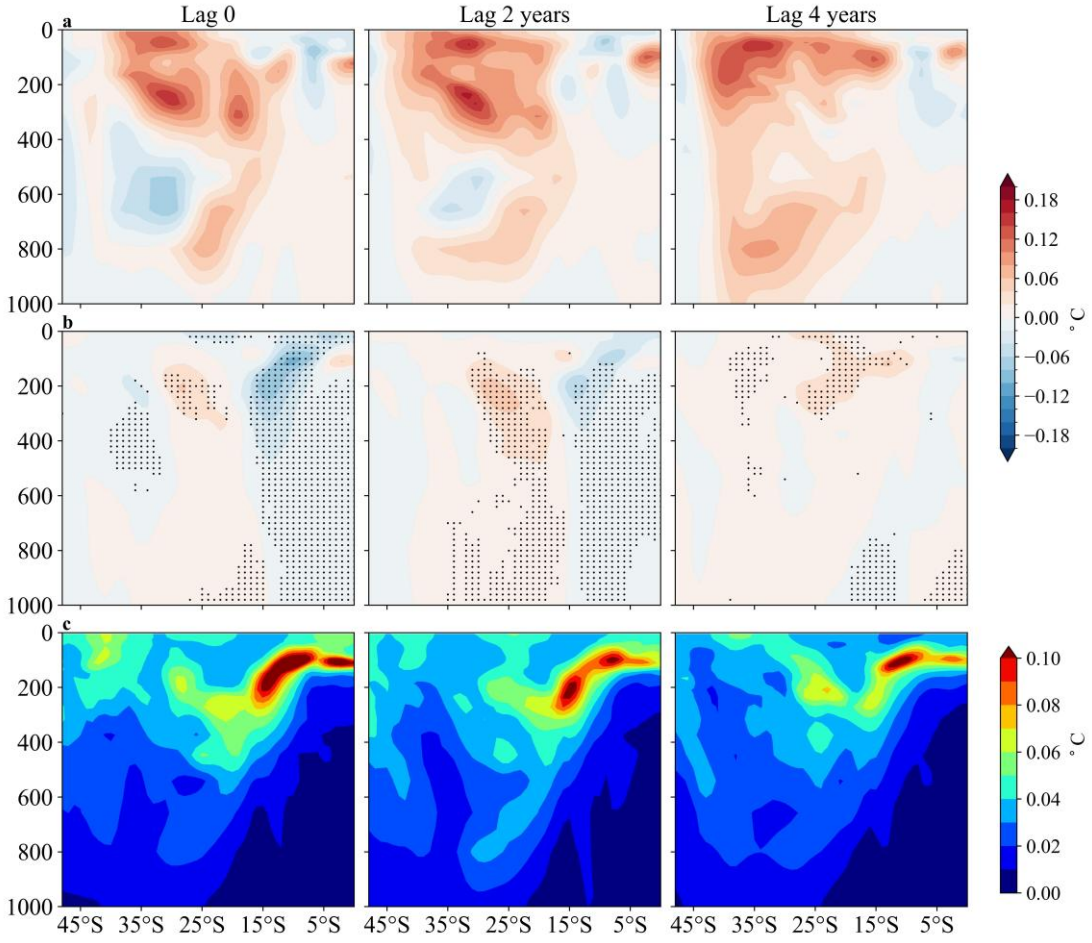


Figure 7: (a) Regression of standardized and detrended decadal ITF to detrended decadal zonally averaged temperature over 45–115°E at zero lag, 2-year and 4-year lag (ITF leads temperature) for ORAS4. (b) Same as (a) but for the multi-model mean of the model ensemble. The stippling indicates the regions where at least 75%

of the models agree on the sign of the regression coefficient. (c) Intermodel spread of the regression coefficients within the ensemble.

These discrepancies may stem from excessive heat loss to the atmosphere in the models or a stronger response to wind-driven convergence. Recent studies (e.g., Sajidh and Chatterjee, 2023; see Figure 1c) report a stronger climatological wind stress curl over the STIO in CMIP6 models. Further, deficiencies in the representation of currents in the SIO might also reduce the skill of models in simulating the accurate distribution of ITF-driven heat.

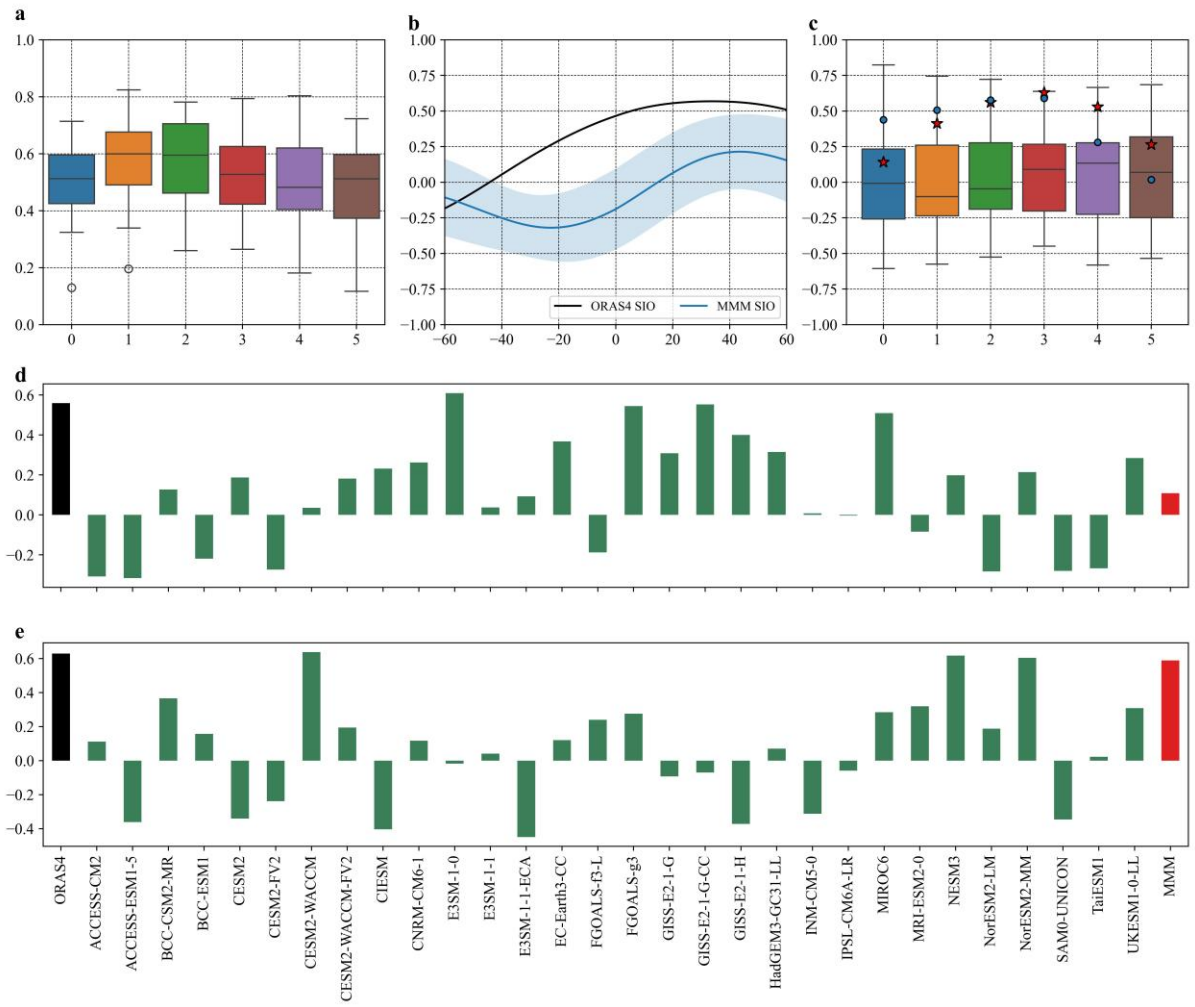


Figure 8: (a) Taylor skill score of regression pattern of decadal ITF h_{700} for ORAS4 with models at different lag (in years) over SIO (45-115°E, 5-40°S). (b) lead lag correlation of the decadal ITF with h_{700} over SIO for different lags (in months), the shading represents the intermodel spread (1 Standard deviation). (c) Pattern correlation of ITF - h_{700} regression to observed long term trend for the models, the same for ORAS4 is marked as stars and the MMM as blue circles. (d) Individual model correlations of (b) at 3-year lead (ITF leads). (e) same as (d) but for (c).

While the influence of the ITF on h_{700} is strongest over the STIO, it is not strictly confined to this region (Figure 5). To facilitate a more robust comparison of spatial heterogeneity, we therefore evaluate the regression patterns over the broader South Indian Ocean (SIO; 5°–40°S). To assess the ability of the models to reproduce the pattern of the ITF–h_{700} regression, we employ a Taylor skill score analysis (see Methods). The median skill score reaches a maximum of approximately 0.6 at a 2-year lag but decreases at both shorter and longer lags (Figure 8a). The relatively low skill at zero lag is directly attributable to the anomalous cooling over the western STIO present in

the models. At longer lags, the decline in skill likely reflects the absence of a southward intensification of the positive h_{700} response in the models (Figure 5c), in contrast to ORAS4 (Figures 5c). In addition, at a lag of 4 years, the models exhibit a weak positive response over the Arabian Sea, with approximately 75% of the models agreeing on the sign of the response (Figure 5c) which is not present in ORAS4. This feature suggests a northward transport of heat which is not present in ORAS4 and may further contribute to the reduced skill score at longer lags.

To assess the evolution of the integrated heat content in the SIO, we calculate the lead–lag correlation between the ITF index and h_{700} integrated over SIO (Figure 8b). ORAS4 correlation shows a peak around 3-4 years of 0.56 while the ensemble mean exhibits considerably lower correlations of ~0.25 at 3-4 years. ORAS4 displays an asymmetric lead–lag structure, characterized by higher correlations at positive lags and weaker, though still positive, correlations at negative lags. In contrast, the MMM shows negative correlations at negative lags, reaching values lower than −0.25.

At a 3-year lag, a few models (e.g., E3SM1-0, GISS-E2-1-G-CC, and FGOALS-g3) show correlations approaching 0.6. A similar analysis over the STIO reveals a comparable lead–lag correlation structure, with only a marginal increase in peak correlations for ORAS4 and the MMM (from ~0.56 to ~0.6) relative to the SIO (not shown).

Since long-term positive trends in the ITF can lead to increased heat uptake in the STIO and influence heat redistribution patterns, we further compare the regression pattern of ITF–h_{700} with the observed long-term trend pattern of h_{700} over the southern Indian Ocean (SIO) (Figure 8c). In ORAS4, the pattern correlation peaks at around a 3-year lag with a value of 0.6, indicating a possible link between ITF variability and long-term subsurface heat distribution in the southern basin. In contrast, pattern correlations in the models remain between −0.2 and 0.2, with a consistent spread across all lags. Analysis of individual model performance shows that although some models perform well in capturing the variability of integrated heat content (e.g., CESM2-WACCM, NorESM2-MM, and NESM3), their pattern correlation with the long-term trends remains poor (Figure 7d, e). This disparity suggests that even when the temporal evolution of integrated heat content is reasonably simulated, it does not necessarily imply that the spatial distribution of warming is realistically captured.

It is clear that models exhibit major deficiencies and a large inter-model spread in representing ITF-driven heat content variability in the STIO. Since the ITF is primarily driven by the Indo-Pacific pressure gradient and Pacific winds, an accurate representation of Pacific-driven variability in the ITF and its role in subsurface heat evolution in the STIO is crucial. Recent studies project a weakening of the ITF under future climate scenarios (Stellama et al., 2019), driven by changes in Pacific and Atlantic forcing, highlighting the importance of understanding how models simulate the ITF–Pacific connection and the subsequent response in the STIO. The next section addresses this by evaluating the representation of Pacific drivers of ITF variability and their role in subsurface heat content evolution in the STIO.

3.3 Linkage and uncertainty in the ITF-Pacific-STIO relationship.

The decadal variability of the ITF has been shown to be closely associated with decadal modulations of climate modes in the Pacific (Li et al., 2018). Accordingly, an accurate representation of Pacific low-frequency variability in models is essential for assessing their ability to simulate inter-basin linkages mediated by the ITF. Prior to evaluating model performance, we perform an Empirical Orthogonal Function (EOF) analysis of Pacific SST using HadISST to isolate the dominant modes of decadal variability, which serves as an observational reference for model evaluation.

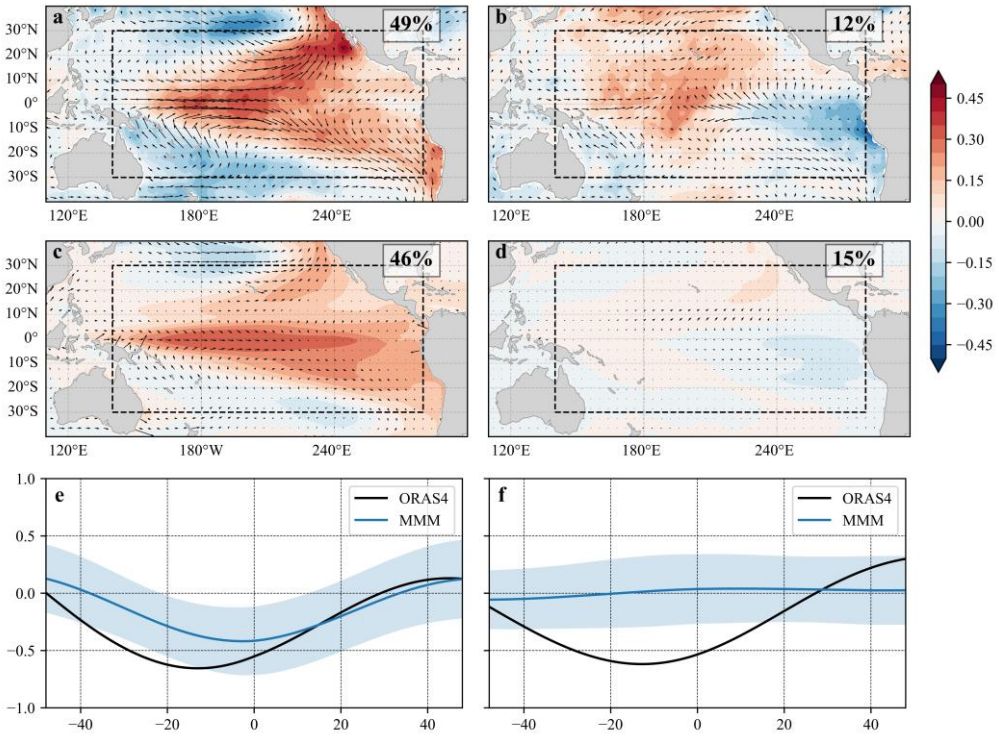


Figure 9: (a) PC1 of decadal SST (140-280°E, 30°S-30°N; dashed black box) regressed to SST and windstress for Observations. (b) same as a but for PC2 for observations. (c) same as (a) but for the MMM. (d) same as (c) but for PC2. (e) lead lag regression of decadal ITF with PC1 for ORAS4 and MMM, the shading represents the intermodel spread (1 SD). (f) same as (e) but for PC2.

The data are linearly detrended over the period 1900–2014 and subsequently filtered with a 7-year low-pass filter to suppress interannual variability and isolate decadal time scales prior to applying EOF analysis. The regression of SST and winds (ERA5) onto the first two principal components (PC1) from the EOF of SST reveals canonical ENSO and ENSO Modoki patterns, respectively, characterized by eastern and central Pacific warming (Figure 9a, b). From here onward, we refer to PC1 as the Niño index and PC2 as the Modoki index and are used for characterising the major modes of decadal variability in the Pacific. Since EOF modes have arbitrary signs, we standardize model indices by enforcing a positive correlation with corresponding area-averaged SST anomaly-based Niño and Modoki indices (see methods) before computing MMM.

We perform a similar analysis on models and note that they generally capture the first mode of variability well, although the regressed winds both in equatorial and off-equatorial regions are notably weaker than for the HadISST-based EOFs (Figure 9c). The first mode explains about 46 ± 10% (Figure S3) of variance in models compared to 49% for observations. While most models reasonably capture the magnitude of the explained variance, a subset of models (e.g., ACCESS-ESM1-5, CESM2-WACCM, and UKESM-1-0-LL) exhibit a higher contribution from the first mode, with explained variance approaching 60%. NorESM2-MM stands out in particular, with the first mode accounting for nearly 75% of the total variance, indicating an unusually dominant leading mode in this model. However, the second mode is poorly represented: the models miss the central Pacific warming and show virtually no associated wind response. The explained variance of the second mode is 15% in observations, but only 12 ± 4 % in the MMM.

To assess the effect of these decadal modes on the ITF, we perform lead–lag correlations between the Niño and Modoki indices and the ITF, using indices and ITF derived from ORAS4 and, separately, from each model, with the indices leading or lagging the ITF. The correlation reaches a maximum of -0.6 when the Nino index lags by

approximately one year and becomes ~0.1 at a lead of ~3 years (Figure 9e), showing an asymmetric response to Nino index. This may reflect a skewed response of ITF to La-Nina compared to El-Nino. In contrast, the MMM shows a maximum correlation near zero lag with a symmetric lead-lag response suggesting that models do not capture the skewed relation between Nino index and ITF observed in ORAS4. For the Modoki index, ORAS4 shows a similar pattern to the Niño index, with an asymmetric lead–lag correlation that peaks when the Modoki index lags the ITF by approximately one year, indicating a significant role in the evolution of the ITF (Figure 6f). In contrast, the models largely miss this relationship, exhibiting near-zero correlations across all leads and lags (Figure 9f), underscoring a general shortcoming of models in simulating the second mode and its associated ITF variability.

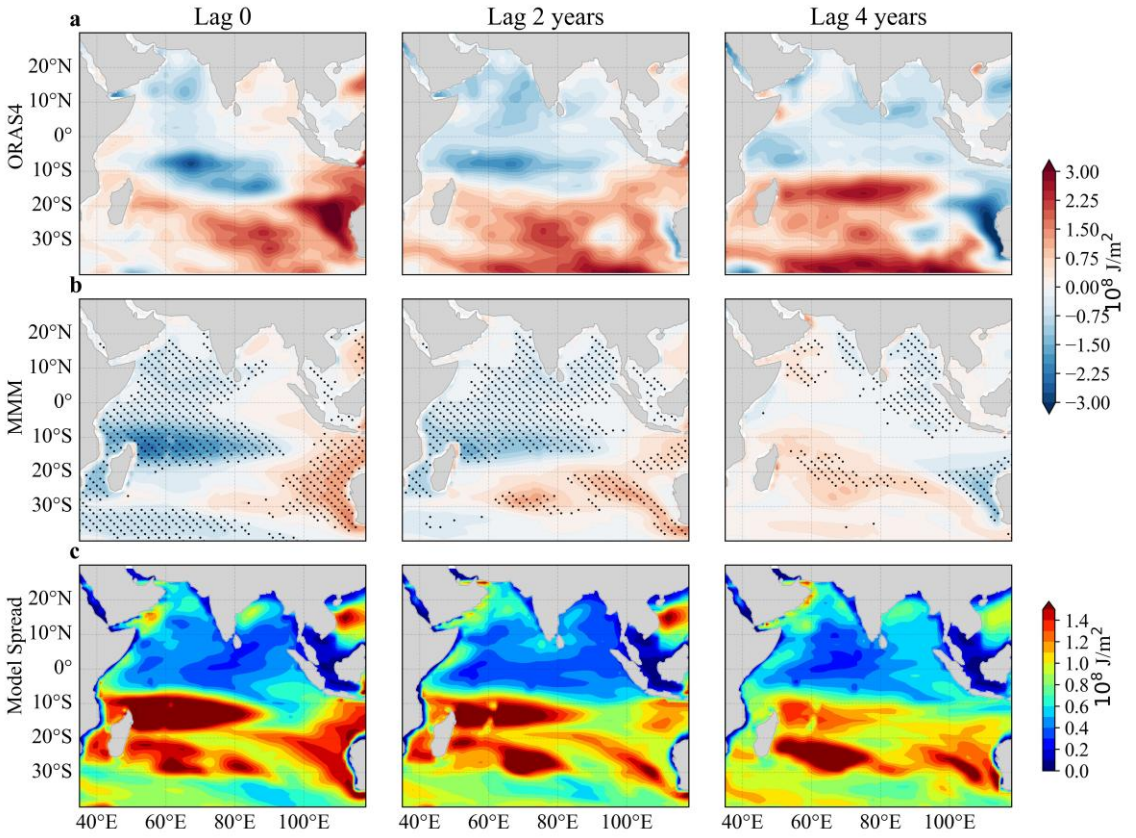


Figure 10: (a) regression of linear regression model of ITF to detrended decadal h_{700} at zero lag, 2 year and 4 year lag (ITF leads h_{700}) for ORAS4. (b) same as a but for the MMM of the model ensemble, the stippling indicates the regions where at least 75% of the models agree on the sign of the regression coefficient. (c) Intermodel spread of the regression coefficients within the ensemble.

We next quantify the combined contribution of Pacific decadal variability to the ITF by constructing a linear reconstruction based on the Niño and Modoki indices. Specifically, the ITF index is regressed separately onto the Niño and Modoki indices, yielding two linear components that represent the individual contributions of the first and second modes of Pacific decadal variability to the ITF. These two components are then linearly combined to form a single reconstructed ITF time series, hereafter referred to as ITF-PAC, which represents the portion of ITF variability associated with Pacific low-frequency variability in ORAS4 and models. Since the Niño and Modoki indices are principal components derived from an EOF analysis of decadal Pacific SSTs, they are orthogonal by construction, ensuring that their contributions to ITF-PAC are linearly independent.

Assessing the correlation between ITF-PAC and the actual ITF time series shows that ORAS4 exhibits a maximum correlation of 0.8 when ITF-PAC lags the ITF by approximately one year (Figure S4), with the expected skewness

also evident in the correlations between the climate mode indices and the ITF discussed previously (Figure 6e,f). In contrast, the models show an approximately instantaneous correlation of ~0.5 with no evident skewness. Notably, models such as CIESM, CNRM-CM6-1, IPSL-CM6A-LR, MIROC6, and NorESM2-MM exhibit stronger correlations than ORAS4. Given the poor representation of the second mode in most models, these stronger correlations reflect an over-dominance of ENSO-related variability.

To compare the response of STIO-h_{700} to ITF-PAC, and in turn assess the Pacific influence, we repeat the regression analysis from Section 2.2 where h_{700} was regressed with ITF at different lag/lead. Here ITF-PAC is used instead of the original ITF time series for both ORAS4 and the models. The ITF-PAC - h_{700} regressions share a comparable spatial structure and westward propagation of positive signal across lags in both ORAS4 and the MMM, albeit with some notable differences.

The major difference is that in the ITF-PAC vs h_{700} regression ORAS4 shows a more pronounced negative response in the western STIO, this suggests the regression model based on the Nino and Modoki indices captures the associated atmospheric teleconnections more effectively (Figure 10a, b). For the models the regression patterns remain mostly the same (Figure 10a, b). To assess how well the ITF-PAC – h_{700} regression reproduces the spatial pattern of the ITF – h_{700} regression from Section 2, we calculated Taylor skill scores (see methods) relative to the ITF–h_{700} regression, which quantify the similarity between the two regression fields. ORAS4 exhibits a skill score of 0.5, increasing to 0.6 at a 3-year lag. Over half of the models achieve scores above 0.5, with some reaching up to 0.95 (Figure S5b-d).

In the models, ITF-PAC exhibits a stronger coupling to STIO heat content compared with ORAS4. The inter-model spread remains comparable between the ITF - h_{700} and ITF-PAC – h_{700} regressions (Figure 10c), underscoring the role of Pacific-origin variability in driving uncertainties in the subsurface heat evolution of the STIO. A recent study by Li et al. (2025) suggests that Indian Ocean winds modulate the ITF depending on the phase of ENSO and IOD events. Hence, the stronger-than-observed Pacific influence in models may indicate deficiencies in how winds are represented during ENSO and IOD phases which in turn diminishes the Indian Ocean influence.

3.4 Model fidelity in capturing long term trends in the Pacific.

Changes in the Pacific Ocean can strongly modulate climate signals in the Indian Ocean (Lee et al., 2015; Kajtar et al., 2015). For instance, the long-term subsurface cooling observed in the tropical Indian Ocean has been partly attributed to the propagation of negative temperature anomalies from the Pacific (Schwarzkopf and Böning, 2011; Ummenhofer et al., 2017). Long-term changes in sea surface temperature (SST), sea level, and surface winds over the Pacific Ocean can exert a significant influence on both the Indian Ocean and the global climate system. For example, the global warming hiatus was linked to sustained cooling in the Pacific, which led to the transport and sequestration of heat into the Indian Ocean (Kosaka et al., 2013; Trenberth and Fasullo, 2013; England et al., 2014). Therefore, an accurate representation of long-term Pacific trends in climate models is essential for reliably simulating Pacific-driven climate signals in the Indian Ocean.

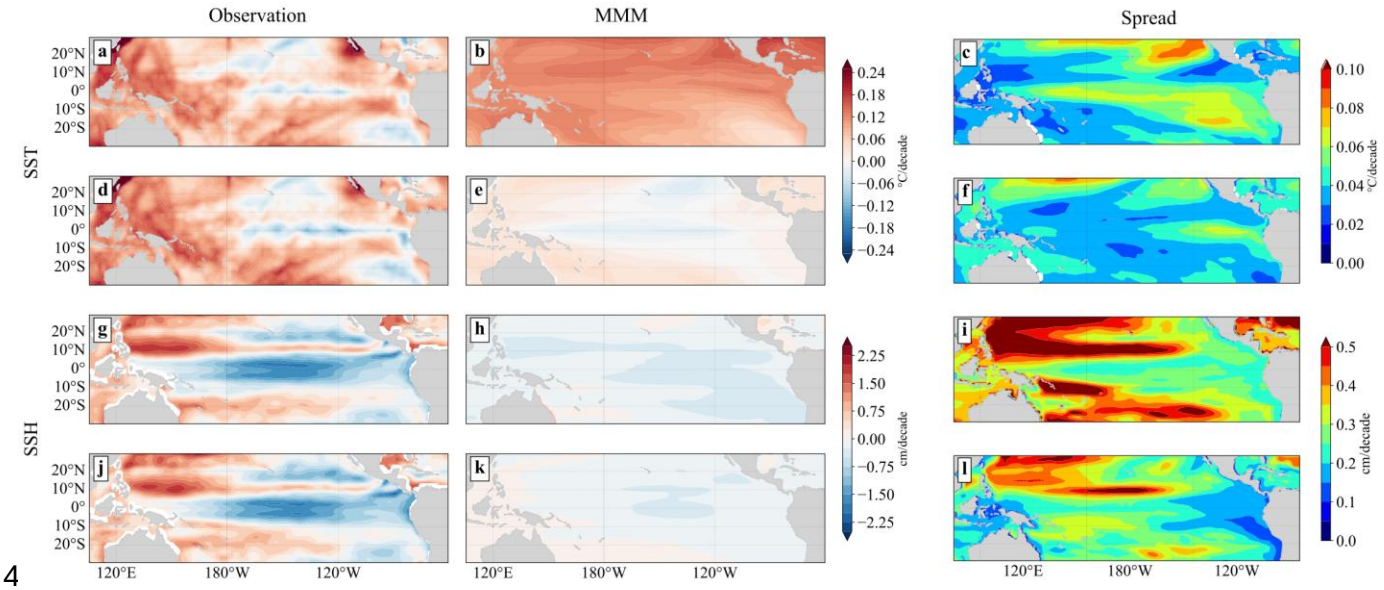


Figure 11: (a) Trend of SST for the period 1960-2014 for observation. (b) same as (a) but for the MMM. (c) Intermodel spread of the h_{700} trends within the ensemble. (d)-(f) same as (a)-(b) but after removing internal variability at decadal scales. (g)-(i) same as (a)-(f) but for sea level.

The observed SST trend shows persistent warming across much of the tropical Pacific, with localized cooling in the equatorial Pacific and regions to its north (Figure 11a). Given the prominence of internal variability on decadal time scales in the Pacific, estimates of long-term trends may be influenced by low-frequency climate modes. To assess the contribution of internal variability, we remove the linearly regressed SST components associated with the Niño and Modoki indices prior to calculating linear trends. Because these indices are derived from an EOF analysis performed on detrended, low-pass–filtered SST anomalies, their removal does not affect the underlying long-term forced trend. The resulting residual SST field is referred to as the forced signal, while the original SST field is referred to as the total signal. Notably, the trend in the forced signal closely resembles that of the total signal in observations, consistent with previous findings (Jiang et al., 2024).

A similar analysis of SST trends in the ensemble reveals clear differences from the observations (Figure 11b,e). The total signal trend in the ensemble exhibits basin-wide warming with no cooling signatures, whereas the forced trend shows equatorial cooling and weaker warming elsewhere (Figure 11b). This pattern resembles an El Niño–like structure in the MMM (Figure 9c), suggesting that an overly strong amplitude of internal variability associated with ENSO and ENSO Modoki in the models biases the estimated long-term trends. Consistent with this interpretation, the intermodel spread is substantially reduced in the forced ensemble, indicating a diminished influence of internal variability in the tropical Pacific (Figure 11,c,f).

Observed sea level trends also show minimal differences between the total and forced signals, characterized by a strong sea level drop in the equatorial Pacific and a rise in the western Pacific (Figure 11g,j). The sea level in the western pacific is a key driver of the pressure gradient between the Pacific and Indian Oceans, which in turn modulates the ITF. The forced signal in the MMM shows a reduced sea level fall and a small positive trend in the western Pacific, compared to a basin-wide fall in the total signal. Notably, the intermodel spread is largest in the western Pacific in the total trends, but this is significantly reduced in the forced trend ensemble (Figure 10i, l).

Zonal wind trends also show large differences in off-equatorial regions with substantial intermodel spread (Figure S6). Notably, both the total and forced trends show relatively weaker amplitudes, indicating model deficiencies in capturing long-term anthropogenic climate signals.

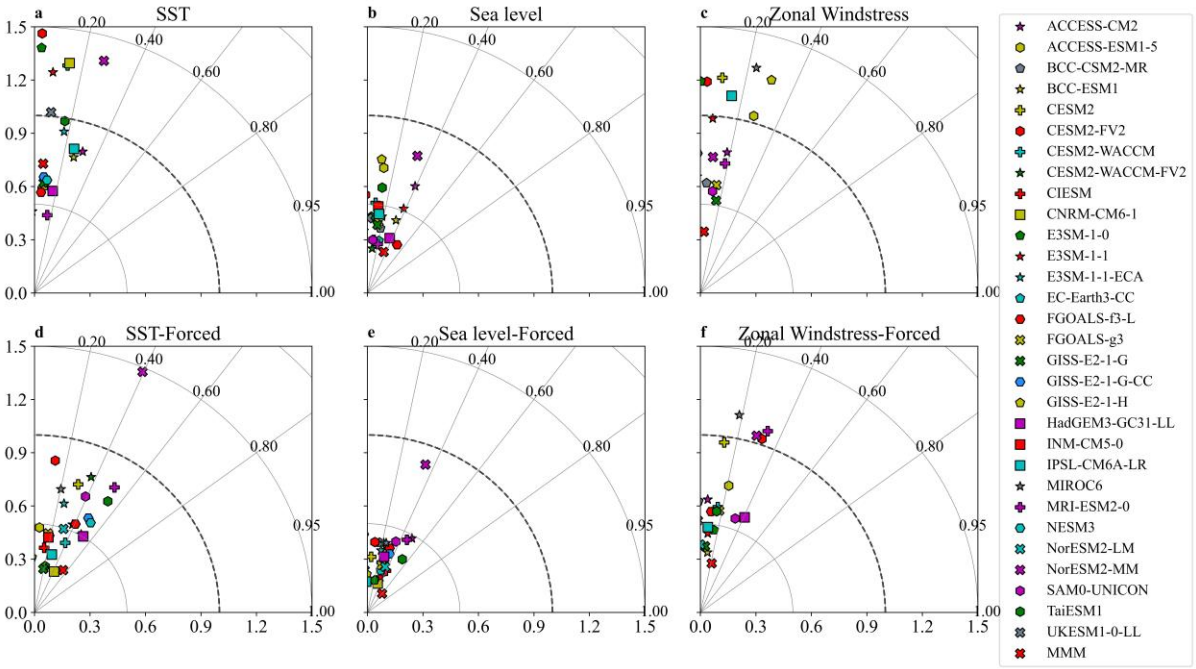


Figure 12: (a) Taylor diagram for SST trend over 1960-2014 for observation and CMIP6 models. (b) same as (a) but for Sea level . (c) same as (a) but for zonal windstress. (d)-(f) same as (a)-(c) for trends over 1960-2014 after removing internal variability at decadal scale.

We use a Taylor skill score analysis to assess model performance in simulating both the total and forced trends in SST, sea level, and zonal wind stress (Figure 12). The models exhibit a large spread in their ability to reproduce the observed spatial patterns of the total SST trend, with maximum pattern correlations reaching ~0.3, and several models showing weak or even negative correlations (Figure 12a). Notably, the skill in simulating the forced SST trends is higher, with approximately ten models exhibiting pattern correlations exceeding 0.4, compared to a maximum of ~0.3 for the total trend. Similar improvements are evident for sea level and zonal wind stress.

These results indicate that, in a substantial number of models, low-frequency internal variability obscures the forced climate signal. However, this interpretation must be treated with care. The apparent masking may reflect either genuinely strong internal variability or the possibility that the externally forced signal has not yet clearly emerged above the background variability. Distinguishing between these two explanations requires further, targeted analysis. Nevertheless, the results suggest that many models struggle to represent the timing of emergence of the forced climate signal accurately. This has important implications for model-based projections. Projections from these models should therefore be interpreted with caution in the STIO, where remotely forced Pacific influences strongly shape subsurface heat content and ITF-related variability.

4 Discussion and conclusions

In this study, we examine the subsurface heat evolution associated with ITF, its linkages to the Pacific Ocean, and its potential role in driving intermodel uncertainties in long-term subsurface heat uptake in STIO within CMIP6 models. Our analysis was motivated by an unusually large spread in the h_{700} trends over the STIO, where the intermodel spread is nearly twice the multi-model mean. Notably, around one-third of the models show zero or negative trends in this region, a marked contrast to the warming pattern present in re-analysis. This conspicuous disagreement prompted a closer look at the processes governing heat transport into the region.

The major focus of our analysis was the relationship between the ITF and the ITF-driven STIO subsurface heat content. While the ITF is widely recognized as a major conduit for Pacific–Indian Ocean exchange, its influence

in modulating sub-surface heat content varies significantly across models. We examine the response of the STIO h_{700} to ITF in models and reanalysis on decadal scales to evaluate mean model behaviors and inter-model disagreements.

Regression analyses at different lags reveal that models exhibit a weak response of h_{700} to ITF variability, although the westward propagation of the signal is retained. In contrast to the reanalysis, where subsurface temperature anomalies show a southward shift in the warming core, models display a more diffuse heat distribution across meridional bands. This weak response in models may stem from several factors, including deficiencies in the background ocean circulation, excessive heat loss to the atmosphere, or overly strong coupling with wind-driven heat redistribution. Additionally, the intermodel spread in the h_{700} response is substantial, nearly three times the magnitude of the multi-model mean response, indicating a lack of consistency in how models simulate the ITF-subsurface heat linkage.

Since the Pacific exerts a strong influence on the variability of ITF, we assess the Pacific control on the ITF by constructing a linear regression model of ITF variability (ITF-PAC) using leading Pacific SST modes and regressing it against h_{700}. This approach revealed that a lot of models outperform the re-analysis with stronger correlations between ITF and ITF-PAC and consequently reproduce ITF-h_{700} regression patterns. This hints at a stronger control of the Pacific on modulating ITF in CMIP6 models.

We also assessed model fidelity in capturing long-term (forced) trends versus total trends in SST, sea level, and wind stress. Many models showed poor agreement with reanalysis in these metrics, suggesting that internal variability continues to mask forced responses in the STIO region. This further highlight the importance of accurately representing the Pacific–Indian Ocean linkages, especially the ITF pathway, to improve confidence in future projections of Indian Ocean subsurface warming.

Looking ahead, climate projections indicate a potential slowdown of the ITF (Sengupta et al., 2016; Stellama et al., 2019). This could significantly alter heat exchange between the Pacific and Indian Oceans, with implications for regional subsurface warming patterns. The intermodel spread in ITF behavior and its influence on the STIO must therefore be carefully addressed. Our study highlights the importance of improving model representation of Indo-Pacific dynamics, especially the processes that govern the strength and variability of the ITF, for better confidence in future projections in the STIO. Accurate representation of the timing of Pacific climate signals is also critical, as misrepresentation of the Time of Emergence may lead to unrealistic inter-basin coupling and contribute to uncertainties in the timing and intensity of subsurface warming in the STIO.

Data Availability

The ORA-S4 reanalysis data are available from the European Centre for Medium-Range Weather Forecasts (ECMWF) at http://www.ecmwf.int/products/forecasts/d/charts/oras4/reanalysis/. CMIP6 model simulation outputs were obtained from the Earth System Grid Federation (ESGF) data portal (https://esgf-node.llnl.gov/projects/esgf-llnl/). The ERA5 wind fields are available from the Copernicus Climate Change Service via https://doi.org/10.24381/cds.f17050d7. Gridded altimeter data were downloaded from the Copernicus Marine Service (https://resources.marine.copernicus.eu/). The HadISST sea surface temperature dataset is provided by the Met Office and is available at https://www.metoffice.gov.uk/hadobs/hadisst/. The codes used for data processing and analysis are available from the corresponding author upon reasonable request.

Acknowledgements

We acknowledge the support provided by the Indian National Centre for Ocean Information Services (INCOIS), Ministry of Earth Sciences(MoES), Govt. of India, to conduct this research. Funding for this work was provided from the “Deep Ocean Mission” programme of the Ministry of Earth Sciences, Government of India.The first author is grateful to CSIR, India for the PhD fellowship, Kerala University of Fisheries and Ocean Studies (KUFOS) for providing the necessary facilities.

Funding

Author SCK received a research fellowship supported by the Council of Scientific and Industrial Research (CSIR), India towards his PhD programme. Funding for this work was provided from the "Deep Ocean Mission" programme of the Ministry of Earth Sciences, Government of India.

Conflict of interest

The authors have no relevant financial or non-financial interests to declare.

Author Contributions

SCK, SJ and AC conceptualized and designed the study. SCK performed the data acquisition, analysis, and figure preparation. SCK drafted the initial version of the manuscript. SJ contributed to the interpretation of results and assisted in drafting and revising the manuscript through scientific discussions. AC provided overall supervision, contributed to the interpretation of the results, and critically revised the manuscript. All authors reviewed and approved the final version of the manuscript.

References

A. Sen Gupta, S. McGregor, E. Van Sebille, A. Ganachaud, J.N. Brown, A. Santoso, Future changes to the Indonesian Throughflow and Pacific circulation: the differing role of wind and deep circulation changes, Geophys. Res. Lett., 43 (4) (2016), pp. 1669-1678

Alory, G., S. Wijffels, and G. Meyers. 2007. "Observed Temperature Trends in the Indian Ocean Over 1960–1999 and Associated Mechanisms." Geophysical Research Letters 34, no. 2: 2–7. https://doi.org/10.1029/2006GL028044.

Anthony G. Bamston, Muthuvel Chelliah & Stanley B. Goldenberg (1997), Documentation of a highly ENSO-related sst region in the equatorial pacific: Research note, Atmosphere-Ocean, 35:3, 367-383, DOI: 10.1080/07055900.1997.9649597

Ashok, K., S. K. Behera, S. A. Rao, H. Weng, and T. Yamagata (2007), El Niño Modoki and its possible teleconnection, J. Geophys. Res., 112, C11007, doi:10.1029/2006JC003798.

Bagnell, A., DeVries, T. 20th century cooling of the deep ocean contributed to delayed acceleration of Earth's energy imbalance. Nat Commun 12, 4604 (2021). https://doi.org/10.1038/s41467-021-24472-3

Balmaseda, M. A., K. Mogensen, and A. T. Weaver. 2013. "Evaluation of the ECMWF Ocean Reanalysis System ORAS4." Quarterly Journal of the Royal Meteorological Society 139, no. 674: 1132–1161. https://doi.org/10.1002/QJ.2063.

Bhanu Deepika, P., Mohan, S., & Srinivas, G. (2024). Intercomparison of tropical Indian Ocean circulation in ocean reanalysis and evaluation in CMIP6 climate models. Dynamics of Atmospheres and Oceans, 106. https://doi.org/10.1016/j.dynatmoce.2024.101456

Bhatia, K.T., Vecchi, G.A., Knutson, T.R. et al. Recent increases in tropical cyclone intensification rates. Nat Commun 10, 635 (2019). https://doi.org/10.1038/s41467-019-08471-z

Bindoff NL, Willebrand J, Artale V, Cazenave A, Gregory JM, Gulev S, Hanawa K, Le Quéré C, Levitus S, Nojiri Y, Shum CK, Talley LD, Unnikrishnan AS (2007) Observations: oceanic climate change and sea level. In: Labeyrie L, Wratt D (eds) Climate change 2007: the physical science basis. Cambridge University Press, pp 385–432

Chen, Y., Su, H., Yan, X. H., Zhang, H., & Wang, Y. (2024). Global oceans suffer extreme heatwaves intensifying since the early 21st century: A new comprehensive index. Ecological Indicators, 162, 112069. https://doi.org/10.1016/j.ecolind.2024.112069

Cheng L, Trenberth KE, Fasullo J, Boyer T, Abraham J, Zhu J. Improved estimates of ocean heat content from 1960 to 2015. Sci Adv. 2017 Mar 10;3(3):e1601545. doi: 10.1126/sciadv.1601545. PMID: 28345033; PMCID: PMC5345929.

Cheng, L., von Schuckmann, K., Abraham, J.P. et al. Past and future ocean warming. Nat Rev Earth Environ 3, 776–794 (2022). https://doi.org/10.1038/s43017-022-00345-1

Church, J.A., P.U. Clark, A. Cazenave, J.M. Gregory, S. Jevrejeva, A. Levermann, M.A. Merrifield, G.A. Milne, R.S. Nerem, P.D. Nunn, A.J. Payne, W.T. Pfeffer, D. Stammer and A.S. Unnikrishnan, 2013: Sea Level Change. In: Climate Change 2013: The Physical Science Basis. Contribution of Working Group I to the Fifth Assessment Report of the Intergovernmental Panel on Climate Change [Stocker, T.F., D. Qin, G.-K. Plattner, M. Tignor, S.K. Allen, J. Boschung, A. Nauels, Y. Xia, V. Bex and P.M. Midgley (eds.)]. Cambridge University Press, Cambridge, United Kingdom and New York, NY, USA.

Church JA, White NJ (2011) Sea-Level Rise from the Late 19th to the Early 21st Century. Surv Geophys 32:585–602. https://doi.org/10.1007/s10712-011-9119-1

Deepa, J.S., Gnanaseelan, C., Kakatkar, R., Parekh, A. and Chowdary, J.S. (2018), The interannual sea level variability in the Indian Ocean as simulated by an Ocean General Circulation Model. Int. J. Climatol, 38: 1132-1144. https://doi.org/10.1002/joc.5228

Dong, L., & McPhaden, M. J. (2017). Why has the relationship between Indian and Pacific Ocean decadal variability changed in recent decades? Journal of Climate, 30(6). https://doi.org/10.1175/JCLI-D-16-0313.1

Duan, J., Y. Li, L. Cheng, P. Lin, and F. Wang, 2023: Heat Storage in the Upper Indian Ocean: The Role of Wind-Driven Redistribution. J. Climate, 36, 2221–2242, https://doi.org/10.1175/JCLI-D-22-0534.1.

Easterling, D. R., and M. F. Wehner (2009), Is the climate warming or cooling? Geophys. Res. Lett., 36, L08706, doi:10.1029/2009GL037810.

Emanuel, K. Increasing destructiveness of tropical cyclones over the past 30 years. Nature 436, 686–688 (2005). https://doi.org/10.1038/nature03906

England, M., McGregor, S., Spence, P. et al. Recent intensification of wind-driven circulation in the Pacific and the ongoing warming hiatus. Nature Clim Change 4, 222–227 (2014). https://doi.org/10.1038/nclimate2106

Eyring, V., Bony, S., Meehl, G. A., Senior, C. A., Stevens, B., Stouffer, R. J., & Taylor, K. E. (2016). Overview of the Coupled Model Intercomparison Project Phase 6 (CMIP6) experimental design and organization. Geoscientific Model Development, 9(5), 1937–1958. https://doi.org/10.5194/gmd-9-1937-2016

Feng, M., Zhang, N., Liu, Q. et al. The Indonesian throughflow, its variability and centennial change. Geosci. Lett. 5, 3 (2018). https://doi.org/10.1186/s40562-018-0102-2

Frölicher, T.L., Fischer, E.M. & Gruber, N. Marine heatwaves under global warming. Nature 560, 360–364 (2018). https://doi.org/10.1038/s41586-018-0383-9

Godfrey JS, Golding TJ (1981) The Sverdrup relation in the Indian Ocean, and the effect of Pacific-Indian Ocean throughflow on the Indian Ocean circulation and on the East Australian Current. J Phys Ocean 11:771–779. https://doi.org/10.1175/1520-0485(1981)011<0771:TSRITI>2.0.CO;2

Godfrey JS (1996) The effect of the Indonesian throughflow on ocean circulation and heat exchange with the atmosphere: a review. J Geophys Res 101:12217–12237. https://doi.org/10.1029/95JC03860

Gordon AL (2005) Oceanography of the Indonesian Seas and their throughflow. Oceanography 18:14–27. https://doi.org/10.5670/oceanog.2005.01

Gregory JM, Griffies SM, Hughes CW, Lowe JA, Church JA, Fukimori I, Gomez N, Kopp RE, Landerer F, le Cozannet G, Ponte RM, Stammer D, Tamisiea ME, van de Wal RSW (2019) Concepts and terminology for sea level: mean, variability and change, both local and global. Surv Geophys. https://doi.org/10.1007/s10712-019-09525-z

Griffies SM, Danabasoglu G, Durack PJ et al (2016) OMIP contribution to CMIP6: experimental and diagnostic protocol for the physical component of the Ocean Model Intercomparison Project. Geosci Model Dev. https://doi.org/10.5194/gmd-9-3231-2016

Gulev, S. K. et al. Changing state of the climate system. Climate Change 2021: The Physical Science Basis. Contribution of Working Group I to the Sixth Assessment Report of the Intergovernmental Panel on Climate Change, 287–422 (Cambridge Univ. Press, 2021).

Halder, S., Parekh, A., Chowdary, J. S., Gnanaseelan, C., & Kulkarni, A. (2021). Assessment of CMIP6 models' skill for tropical Indian Ocean sea surface temperature variability. International Journal of Climatology, 41(4), 2568–2588. https://doi.org/10.1002/joc.6975

Han W, Meehl GA, Rajagopalan B et al (2010) Patterns of Indian Ocean sea-level change in a warming climate. Nat Geosci. https://doi.org/10.1038/ngeo901

Hersbach, H., B. Bell, P. Berrisford, et al. 2020. "The ERA5 Global Reanalysis." Quarterly Journal of the Royal Meteorological Society 146, no. 730: 1999–2049. https://doi.org/10.1002/QJ.3803.

Hirst AC, Godfrey JS (1993) The role of Indonesian throughflow in a Global Ocean GCM. J Phys Oceanogr 23:1057–1086. https://doi.org/10.1175/1520-0485(1993)023<1057:TROITI>2.0.CO;2

Hunt, B.G. The role of natural climatic variation in perturbing the observed global mean temperature trend. Clim Dyn 36, 509–521 (2011). https://doi.org/10.1007/s00382-010-0799-x

Hu S., Zhang Y., Feng M., Du Y., Sprintall J., Wang F., et al. (2019). Interannual to decadal variability of upper-ocean salinity in the southern Indian ocean and the role of the Indonesian throughflow. J. Climate 32 (19), 6403–6421. doi: 10.1175/JCLI-D-19-0056.1

IPCC. Climate Change 2021: The Physical Science Basis. Contribution of Working Group I to the Sixth Assessment Report of the Intergovernmental Panel on Climate Change (eds Masson-Delmotte, V. et al.) (Cambridge Univ. Press, 2021)

Jiang, F., Seager, R. & Cane, M.A. A climate change signal in the tropical Pacific emerges from decadal variability. Nat Commun 15, 8291 (2024). https://doi.org/10.1038/s41467-024-52731-6

Jin, X., Kwon, Y. O., Ummenhofer, C. C., Seo, H., Schwarzkopf, F. U., Biastoch, A., Böning, C. W., & Wright, J. S. (2018). Influences of pacific climate variability on decadal subsurface Ocean heat content variations in the Indian Ocean. Journal of Climate, 31(10), 4157–4174. https://doi.org/10.1175/JCLI-D-17-0654.1

Jin, X., Kwon, Y. O., Ummenhofer, C. C., Seo, H., Kosaka, Y., & Wright, J. S. (2018). Distinct mechanisms of decadal subsurface heat content variations in the eastern and western Indian Ocean modulated by tropical Pacific SST. Journal of Climate, 31(19), 7751–7769. https://doi.org/10.1175/JCLI-D-18-0184.1

Kajtar, J. B., A. Santoso, M. H. England, and W. Cai, 2015: Indo-Pacific Climate Interactions in the Absence of an Indonesian Throughflow. J. Climate, 28, 5017–5029, https://doi.org/10.1175/JCLI-D-14-00114.1.

Kennedy, J., Folland, C. K., Palmer, M. D., & Parker, D. (2009). Do global temperature trends over the last decade falsify climate predictions? Bulletin of the American Meteorological Society, 90(8).

Kharin, V. V., Zwiers, F. W., Zhang, X., & Wehner, M. (2013). Changes in temperature and precipitation extremes in the CMIP5 ensemble. Climatic Change, 119(2), 345–357. https://doi.org/10.1007/s10584-013-0705-8

Kosaka, Y., Xie, SP. Recent global-warming hiatus tied to equatorial Pacific surface cooling. Nature 501, 403–407 (2013). https://doi.org/10.1038/nature12534

Lee, SK., Park, W., Baringer, M. et al. Pacific origin of the abrupt increase in Indian Ocean heat content during the warming hiatus. Nature Geosci 8, 445–449 (2015). https://doi.org/10.1038/ngeo2438

Lee T, Fukumori I, Menemenlis D et al (2002) Effects of the Indonesian throughflow on the Pacific and Indian oceans. J Phys Oceanogr 32:1404–1429. https://doi.org/10.1175/1520-0485(2002)032<1404:Eotito>2.0.Co;2

Li, M., Gordon, A. L., Wei, J., Gruenburg, L. K., & Jiang, G. (2018). Multi-decadal timeseries of the Indonesian throughflow. Dynamics of Atmospheres and Oceans, 81, 84–95. https://doi.org/10.1016/j.dynatmoce.2018.02.001

Li, R., Li, Y., Lyu, Y., Sprintall, J., & Wang, F. (2025). Role of the Indian Ocean wind-driven dynamics in the Indonesian Throughflow variability. Journal of Geophysical Research: Oceans, 130, e2025JC022503. https://doi.org/10.1029/2025JC022503

Li M., Gordon A. L., Wei J., Gruenburg L. K., Jiang G. (2018). Multi-decadal timeseries of the Indonesian throughflow. Dynamics Atmospheres Oceans 81, 84–95. doi: 10.1016/j.dynatmoce.2018.02.001

Macdonald A (1993) Property fluxes at 30°S and their implications for the Pacific-Indian throughflow and the global heat budget. J Geophys Res 98:6851–6868. https://doi.org/10.1029/92JC02964

Madan, G., Gjermundsen, A., Iversen, S.C. et al. The weakening AMOC under extreme climate change. Clim Dyn 62, 1291–1309 (2024). https://doi.org/10.1007/s00382-023-06957-7

Mayer, M., Alonso Balmaseda, M., & Haimberger, L. (2018). Unprecedented 2015/2016 Indo-Pacific heat transfer speeds up tropical Pacific heat recharge. Geophysical Research Letters, 45, 3274–3284. https://doi.org/10.1002/2018GL077106

Meehl, G. A., A. Hu, J. M. Arblaster, J. Fasullo, and K. E. Trenberth, 2013: Externally Forced and Internally Generated Decadal Climate Variability Associated with the Interdecadal Pacific Oscillation. J. Climate, 26, 7298–7310, https://doi.org/10.1175/JCLI-D-12-00548.1.

Meyssignac, B. et al. Measuring global ocean heat content to estimate the Earth energy imbalance. Front. Mar. Sci. 6, 432 (2019).

Oldenburg, D., Y. Kwon, C. Frankignoul, G. Danabasoglu, S. Yeager, and W. M. Kim, 2024: The Respective Roles of Ocean Heat Transport and Surface Heat Fluxes in Driving Arctic Ocean Warming and Sea Ice Decline. J. Climate, 37, 1431–1448, https://doi.org/10.1175/JCLI-D-23-0399.1.

P. J. Webster et al. ,Changes in Tropical Cyclone Number, Duration, and Intensity in a Warming Environment.Science309,1844-1846(2005).DOI:10.1126/science.1116448

Pontes, G.M., Menviel, L. Weakening of the Atlantic Meridional Overturning Circulation driven by subarctic freshening since the mid-twentieth century. Nat. Geosci. 17, 1291–1298 (2024). https://doi.org/10.1038/s41561-024-01568-1

Qu T, Meyers G, Godfrey JS, Hu D (1994) Ocean dynamics in the region between Australia and Indonesia and its influence on the variation of sea surface temperature in a global general circulation model. J Geophys Res 99:18433–18445. https://doi.org/10.1029/94JC00858

Rantanen, M., A. Y. Karpechko, A. Lipponen, K. Nordling, O. Hyvärinen, K. Ruosteenoja, T. Vihma, and A. Laaksonen, 2022: The Arctic has warmed nearly four times faster than the globe since 1979. Commun. Earth Environ., 3, 168, https://doi.org/10.1038/s43247-022-00498-3.

Rayner, N. A., D. E. Parker, E. B. Horton, C. K. Folland, L. V. Alexander, D. P. Rowell, E. C. Kent, and A. Kaplan (2003), Global analyses of sea surface temperature, sea ice, and night marine air temperature since the late nineteenth century, J. Geophys. Res., 108, 4407, doi:10.1029/2002JD002670, D14.

Richard A. Kerr ,What Happened to Global Warming? Scientists Say Just Wait a Bit.Science326,28-29(2009).DOI:10.1126/science.326_28a

Roemmich, D., Church, J., Gilson, J. et al. Unabated planetary warming and its ocean structure since 2006. Nature Clim Change 5, 240–245 (2015). https://doi.org/10.1038/nclimate2513

Rosen, J. Indian Ocean may be key to global warming 'hiatus'. Nature (2015). https://doi.org/10.1038/nature.2015.17505

Sajidh, C. K., A. Chatterjee, R. Murtugudde, M. J. McPhaden, S. S. C. Shenoi, and P. N. Vinayachandran. 2025. " Rapid 21st Century Warming in the Southern Subtropical Indian Ocean Driven by Altered Inter-Basin Connections." International Journal of Climatology e70157. https://doi.org/10.1002/joc.70157.

Sajidh, C.K., Chatterjee, A. Indian Ocean dynamic sea level, its variability and projections in CMIP6 models. Clim Dyn 61, 2229–2252 (2023). https://doi.org/10.1007/s00382-023-06676-z

Schwarzkopf, F. U., and C. W. Böning (2011), Contribution of Pacific wind stress to multi-decadal variations in upper-ocean heat content and sea level in the tropical south Indian Ocean, Geophys. Res. Lett., 38, L12602, doi:10.1029/2011GL047651.

Sen Gupta, A., S. McGregor, E. van Sebille, A. Ganachaud, J. N. Brown, and A. Santoso (2016), Future changes to the Indonesian Throughflow and Pacific circulation: The differing role of wind and deep circulation changes, Geophys. Res. Lett., 43, 1669–1678, doi:10.1002/2016GL067757.

Sloyan and Rintoul 2001 - Sloyan BM, Rintoul SR (2001) Circulation, renewal, and modification of Antarctic mode and intermediate water. J Phys Oceanogr 31:1005–1030. https://doi.org/10.1175/1520-0485(2001)031<1005:CRAMOA>2.0.CO;2

Song, Y., Li, Y., Forget, G. et al. Inter-basin contrast in the Southern Ocean warming. Nat Commun 16, 9063 (2025). https://doi.org/10.1038/s41467-025-64112-8

Soumya, M. (2025). Role of Indonesian throughflow on Indian Ocean warming pattern formation during the recent global warming hiatus in CMIP6 models. Global and Planetary Change, 253. https://doi.org/10.1016/j.gloplacha.2025.104969

Sprintall J, Gordon AL, Koch-Larrouy A et al (2014) The Indonesian seas and their role in the coupled ocean–climate system. Nat Geosci 7:487–492. https://doi.org/10.1038/ngeo2188

Stellema, A., Sen Gupta, A. & Taschetto, A.S. Projected slow down of South Indian Ocean circulation. Sci Rep 9, 17705 (2019). https://doi.org/10.1038/s41598-019-54092-3

Taylor KE (2001) Summarizing multiple aspects of model performance in a single diagram. J Geophys Res Atmos. https://doi.org/10.1029/2000JD900719

Tebaldi, C., Debeire, K., Eyring, V., Fischer, E., Fyfe, J., Friedlingstein, P., et al. (2021). Climate model projections from the Scenario Model Intercomparison Project (ScenarioMIP) of CMIP6. Earth System Dynamics, 12(1), 253–293. https://doi.org/10.5194/esd-12-253-2021

Trenary, L. L., and W. Han (2008), Causes of decadal subsurface cooling in the tropical Indian Ocean during 1961–2000, Geophys. Res. Lett., 35, L17602, doi:10.1029/2008GL034687.

Trenberth, K. E., and J. T. Fasullo (2013), An apparent hiatus in global warming? Earth's Future, 1(1), 19–32, doi:10.1002/2013ef000165

Trenberth, K. E., J. T. Fasullo, and M. A. Balmaseda, 2014: Earth's Energy Imbalance. J. Climate, 27, 3129–3144, https://doi.org/10.1175/JCLI-D-13-00294.1.

Ummenhofer, C. C., A. Biastoch, and C. W. Böning, 2017: Multidecadal Indian Ocean Variability Linked to the Pacific and Implications for Preconditioning Indian Ocean Dipole Events. J. Climate, 30, 1739–1751, https://doi.org/10.1175/JCLI-D-16-0200.1.

Unnikrishnan AS, Nidheesh AG, Lengaigne M (2015) Sea-level-rise trends off the Indian coasts during the last two decades. Curr Sci 108:966–970

von Schuckmann, K., Cheng, L., Palmer, M. D., Hansen, J., Tassone, C., Aich, V., Adusumilli, S., Beltrami, H., Boyer, T., Cuesta-Valero, F. J., Desbruyères, D., Domingues, C., García-García, A., Gentine, P., Gilson, J., Gorfer, M., Haimberger, L., Ishii, M., Johnson, G. C., Killick, R., King, B. A., Kirchengast, G., Kolodziejczyk, N., Lyman, J., Marzeion, B., Mayer, M., Monier, M., Monselesan, D. P., Purkey, S., Roemmich, D., Schweiger, A., Seneviratne, S. I., Shepherd, A., Slater, D. A., Steiner, A. K., Straneo, F., Timmermans, M.-L., and Wijffels, S. E.: Heat stored in the Earth system: where does the energy go?, Earth Syst. Sci. Data, 12, 2013–2041, https://doi.org/10.5194/essd-12-2013-2020, 2020.

Vranes K, Gordon AL, Ffield A (2002) The heat transport of the Indonesian throughflow and implications for the Indian Ocean heat budget. Deep Res Part II 49:1391–1410. https://doi.org/10.1016/S0967-0645(01)00150-3

Wijffels, S., Roemmich, D., Monselesan, D. et al. Ocean temperatures chronicle the ongoing warming of Earth. Nature Clim Change 6, 116–118 (2016). https://doi.org/10.1038/nclimate2924

Wu, C., Yeh, P. J. F., Ju, J., Chen, Y.-Y., Xu, K., Dai, H., et al. (2021). Assessing the spatiotemporal uncertainties in future meteorological droughts from CMIP5 models, emission scenarios, and bias corrections.

Yang, H., G. Lohmann, U. Krebs-Kanzow, et al. 2020. "Poleward Shift of the Major Ocean Gyres Detected in a Warming Climate." Geophysical Research Letters 47, no. 5: e2019GL085868. https://doi.org/10.1029/2019GL085868.

Zhang, Y., Feng, M., Du, Y., Phillips, H. E., Bindoff, N. L., & McPhaden, M. J. (2018). Strengthened Indonesian Throughflow Drives Decadal Warming in the Southern Indian Ocean. Geophysical Research Letters, 45(12). https://doi.org/10.1029/2018GL078265

Zuo, H., M. A. Balmaseda, S. Tietsche, K. Mogensen, and M. Mayer. 2019. "The ECMWF Operational Ensemble Reanalysis-Analysis System for Ocean and Sea Ice: A Description of the System and Assessment." Ocean Science 15, no. 3: 779–808. https://doi.org/10.5194/OS-15-779-2019.

Supplementary Files

This is a list of supplementary files associated with this preprint. Click to download.

- SupplementaryMaterial.docx